Neutron background measurements in the underground laboratory of Modane

V. Chazal, B. Chambon, M. de Jésus, D. Drain, C. Pastor, L. Vagneron, R. Brissot, J.F. Cavaignac, A. Stutz, Y. Giraud-Heraud

DD

[redacted]

Neutron background measurements in the underground laboratory of Modane

V. CHAZAL[a,*], R. BRISSOT[b], J. F. CAVAIGNAC[b], B. CHAMBON[a,+], M. DE JESUS[a,+], D. DRAIN[a,+], Y. GIRAUD-HERAUD[c], C. PASTOR[a,+], A. STUTZ[b], L. VAGNERON[a,+]

[a] *Institut de Physique Nucléaire de Lyon and Université Claude Bernard, Lyon I, IN2P3 - CNRS, 43 Bd du 11 Novembre 1918, F-69622 Villeurbanne Cedex*

[b] *Institut des Sciences Nucléaires de Grenoble and Université Joseph Fourier, Grenoble, IN2P3 - CNRS, 53 Avenue des Martyrs, F-38026 Grenoble Cedex*

[c] *Laboratoire de Physique Corpusculaire, Collège de France IN2P3 - CNRS, 11 place M. Berthelot, F-75231 Paris Cedex 05*

Abstract

Measurements of the background neutron environment, at a depth of 1780 m (4800 mwe) in the Underground Laboratory of Modane (L.S.M) are reported. Using a ^{6}Li liquid scintillator, the energy spectrum of the fast neutron flux has been determined. Monte-Carlo calculations of the (α,n) and spontaneous fission processes in the surrounding rock has been performed and compared to the experimental result. In addition, using two ^{3}He neutron counters, the thermal neutron flux has been measured.

PACS : 95.35 + d ; 28.20 - V ; 91.65 . Dt

Keywords : Dark matter, Quenching factor, Neutrons, Underground site

* Present address : Institut de Physique, rue A. L. Breguet 1, CH - 2000 Neuchâtel
e mail : verene.chazal@iph.inine.ch Phone : (41) 32 721 19 83 Fax : (41) 32 718 29 01

[+] EDELWEISS Collaboration

1. Introduction

There exist astrophysical observations which suggest that more than 90% of the mass in the universe is in the form of Dark Matter, baryonic [1] or non-baryonic [2]. The EDELWEISS collaboration (Expérience pour DEtecter Les WImps En Site Souterrain) designed a deep underground low radioactivity cryogenic facility devoted to WIMPs (Weakly Interactive Massive Particle) bolometric detection at the Laboratoire Souterrain de Modane (L.S.M) [3].

The expected interaction rate of WIMPs in a crystal is in the order of 10^{-2} evt/ kg/ day [4]. In such an experiment, where the expected event rate is very low, neutrons are a particularly important background source. Neutrons - as WIMPs - induce nuclear recoil, which prevents from an "active" rejection of this background. It is crucial, therefore, that the energetic neutron flux at the experimental site should be measured to determine the appropriate shielding of the future experiments.

The L.S.M is situated in the Alps at the French-Italian border, in the Fréjus highway tunnel. The site offers a 1780 m rock coverage against cosmic radiation (4800 m water equivalent). The measured residual cosmic muon flux is of 4.2 $m^{-2}.day^{-1}$ [5], i.e an attenuation of the surface flux by a factor of $\approx 10^6$.

Several authors have measured the background neutron flux in underground environments. For example in the Gran Sasso (3950 mwe) [6], or in a mine at Broken Hill in Australia (3200 mwe) [7], they measured the thermal, epithermal and fast neutron flux. Moreover in Australia, they studied the origin of the neutrons from the composition of the rock at the experimental site.

In the present paper, we report the result of our measurements of the background neutron flux in the L.S.M. We measured the flux and the energy spectrum of the fast neutrons, using a ^{6}Li-loaded liquid scintillator detector. We also studied the origin of the neutrons in the L.S.M, in order to use the best shielding. Finally to have a complete view of the neutrons in the L.S.M, we measured the flux of thermal neutrons using two ^{3}He detectors.

2. Fast neutron counter and calibration

2.1 Description of the detector

The neutron detection module developed for neutrinos detection by the Bugey collaboration experiment [8] has been adapted. The detector is composed of one parallelepiped cell (80 x 10 x 10 cm^3), instrumented at each side by a photomultiplier. It is

filled with a pseudocumene based liquid scintillator NE320, doped with 0.15% of ^{6}Li (in weight). The materials which are in contact with the liquid are 316L stainless steel and teflon. A metallic shielding of 12 cm of lead and 5 cm of copper protects the detector from external gamma radiation.

We need a very sensitive detector, because of the low neutron / gamma ratio. This detector allows to use the pulse shape discrimination (PSD) properties of the liquid scintillator. The PSD technique requires the optimization of the amount of detected light without too much timing degradation, which imposes the use of total reflection. The detector light guide is described in Ref. [8].

2.2 Detector principles

A fast neutron entering the detector will induce two light pulses (Fig. 1) :

- the slowing down of the neutron through elastic collisions on protons, which gives a prompt signal,
- the thermalized neutron capture pulse (delayed pulse), corresponding to the interaction with a ^{6}Li nucleus.

$$n_{Therm} + {}^6Li \rightarrow \alpha + {}^3H \qquad (Q = 4.8\ MeV)$$

For each event, we measured the total charge Q_1, which is the sum of the right charge Q_R and left charge Q_L, corresponding to each photomultiplier, integrated on a time interval of 500 ns. Q_1 is corrected from the longitudinal variation in the cell.

* The PSD property of the liquid is used by comparing Q_1 with its fraction Q_2 left after typically 20 ns. The ratio $R_{PSD} = \frac{Q_2}{Q_1}$ is independent of the longitudinal localization of the event. It was used for the thermal neutron as well as for the fast neutron identification. Fig. 2 represents the spectrum of the ratio R_{PSD} of the prompt events obtained with neutrons from an Am-Be source.

* L is the localization variable along the cell : $L = \frac{Q_L - Q_R}{Q_L + Q_R}$.

We used a collimated ^{60} Co source, placed in different positions along the detector, to calibrate it in centimeters. L is used for the prompt and delayed interactions.

2.3 Calibration

To calibrate the detector in neutron energy, we have to take into account the quenching effect. The light quantity depends on the particle nature and is not proportional to the deposited energy. Therefore the measurement of the correspondence between light output and energy, which depends on the scintillator, is important. We used monoenergetic neutrons. In the obtained continuous spectrum, the highest light corresponds to a neutron energy loss in a single impact, which is equivalent to a total neutron energy transfer.

The detector response to fast neutrons was studied at the 14 MeV Tandem of the CEN of Bruyères-le-Châtel, via the reaction ^{7}Li (p,n) ^{7}Be. The proton beam impinged on the ^{7}Li target (140 $\mu g/ cm^2$) with proton energies ranging between 3 and 6 MeV. The emitted neutrons strike the scintillator at an angle $\theta = 0° \pm 10°$ ($\Delta\theta$ induced an energy spread of $\Delta E = \pm 20$ keV), relative to the proton beam at a distance of 4.54 m away from target.

For each event, we measured the total charge Q_1, and Q_2. In addition, the following information was recorded :

- Time-Of-Flight (TOF) between the target and the detector, which gives the energy of the neutrons,
- neutron - gamma detector PSD information.

We were able to calibrate the light response of the recoil protons as a function of the neutron energy, for 7 incident protons energies. The energy calibration in electron equivalent energy in the scintillator was done by setting a ^{60}Co source in the middle of the detector.

We studied the spectrum region where all the neutron energy was lost in one impact. From the highest part of the recoil proton energy spectrum, and for each incident neutron energy, we determined the maximal energy transfer in electron equivalent, taking into account the detector resolution (10 %).

We obtained 7 experimental points (corresponding to the 7 incident proton energies). We deduced the light efficiency curve with the Birks' law modified by Chou [9], to obtain the detector calibration in neutron energy.

Figure 3 shows our results compared to measurements with various organic scintillators for which the light response is known [10].

3. Experimental procedure

3.1 Experimental setup and electronics

As quoted in the previous section, a neutron event is defined by two successive light pulses induced by a "prompt" and a "delayed" particle, both well localized in space and time. We have to check for a delayed coincidence between two such particles. The particle identification is done using pulse shape criteria. All logical signals are derived from constant discriminators (DFC) with a typical threshold corresponding to 260 keV electron equivalent energy deposition.

The different steps of the acquisition were :

- the coding of prompt event parameters with a QDC (first pulse). These parameters were the total and delayed charge collected on each photomultiplier which give access to the PSD signature,
- the coding of delayed event parameters (second pulse),
- a TAC measured the delay between the prompt signal and the delayed signal, on a range of 200 μs.

We only kept events made of 2 pulses separated by a time interval lower than 180 μs. These signals are analysed later, with five selection criteria.

3.2 Signatures

Five signatures allow identification of the neutron :

- the shape of the prompt pulse (Fig. 4a). Thanks to good discrimination properties of the liquid, we can perform a high rejection of the γ induced background,
- the PSD analysis of the delayed pulse, allowing the identification of the (α+t) charged particles of ^6Li + n reaction (Fig. 4b),
- the 0.53 MeV electron equivalent energy of the (α+t) delayed pulses (Fig. 4b),
- the time interval (t ≈ 25 μs) between prompt and delayed signal which correspond to the neutron migration time,
- the thermal neutron migration distance. The maximal distance between the recoiling proton and neutron capture is ≈ 20 cm (the mean distance of the thermalization itself is ≈ 6 cm).

3.3 Experimental results

During the experiment, we have used two different mechanical set-ups :

- in a first phase, the detector located inside a shielding of lead and copper (8 months),
- in a second phase, a 30 cm thick wax protection was installed all around the shielding, and 20 cm above the cover (5 months).

Wax moderates and captures a large part of the incoming neutrons. We show by simulation with GEANT [11] that a thickness of wax of 30 cm is sufficient to stop neutrons flux inside the detector [12]. For a mean energy of 3 MeV, only a neutron fraction (0.5 %) crossed the wax shield without absorption.

We found an event rate of (1.15 ± 0.09) evt/ day in the first phase and (0.38 ± 0.06) evt/ day in the second phase in the detector. In the second phase, with 30 cm wax protection all around the shielding, the residual rate obviously does not come from the outside of the shielding. The results showed that the event rate is reduced by a factor 3 with wax.

Figure 5 shows the distribution of the neutron capture times for the first (lead + copper) and second (wax + lead + copper) phase. The mean capture times are respectively 21.7 μs for the first phase and 28 μs for the second phase. These results are coherent with the characteristic time of 25 μs [8].

Figure 6 represents the neutron energy spectrum. This spectrum is displayed in electron equivalent energy, with a threshold effect on the first energy bin.

4. Efficiency corrections and results

To get the true internal neutron rate, we have to take into account the detector efficiency, the losses induced by the electronics, the rejection of the various selection criteria, and the light response of the detector.

4.1 Estimation of analysis cuts efficiency

- the (n - γ) discrimination for prompt events : from the (n - γ) discrimination parameter, a gaussian fit is applied on the neutron peak. A 2σ cut leads to the eliminated neutrons rate (11 %).

- the energy of (α+t) events : this signature leads to a good discrimination of these events. 10 % of the events are rejected by our cut, using an Am-Be source (Fig. 4b).

- the efficiency of the "relative distance" parameter is obtained by the relative localisation spectrum of an Am-Be source. We obtain an efficiency of 70 %.

- the time interval distribution : a time window of $2\tau = 50$ µs is used to eliminate the background of random events. There is also an electronic dead time of 3 µs generated by the processing of the prompt signal. The corresponding delayed events (12 %) are not recorded. We obtain a total efficiency of 76 %.

The results are summarized in table 1.

Signature	Efficiency
recoil protons identification	89 %
(α + t) identification	
(α + t) peak magnitude	90 %
relative distance	70 %
electronic dead time	76 %

Table 1 : Efficiency of each signature

Conclusion : the total losses due to the various cuts are 43 %. It is very difficult to estimate correlations between the five selection criteria used to identify a neutron, so the final result is probably overestimated for all signature efficiency.

* Random events background

The accidental rate is induced mainly by Compton scattering of γ ray. Its estimation is obtained with the prompt events. This rate (5×10^{-3} events per day) is negligible when we compare with the true neutron event rate.

4.2 Monte Carlo simulations : energy spectrum of the incoming neutron

H. de Kerret and B. Lefièvre developed for the Bugey experiment a simulation program for low energy neutrons, based on GEANT, which is well adapted to our experiment [13]. The program is able to track individual neutrons in an energy range of 0.001 eV to 10 MeV, loosing its energy by elastic collisions in the different materials of the detector (scintillator, iron, acrylic, glass, etc...) [8]. We have simulated the slowing down of the neutron inside all materials of the detector, and even outside the detector (wax region) until its thermalization and final capture.

From the experimental spectrum (Fig. 6), we obtained the primary neutron energy spectrum in the laboratory, represented in figure 7. This neutron energy spectrum was the sum

of 9 weighted Dirac deltas. Each delta corresponding to a neutron energy (between 2 and 6 MeV) was introduced in a detector and shielding simulation, and lead to a continuous spectrum. The 9 spectra obtained were weighted and added to fit the experimental spectrum, taking into account the detector efficiency, the electronics losses and the rejection of the various selection criteria.

4.3 Neutron flux in the underground laboratory

From the event rate measured in the first phase (see 3.3 Experimental results), and taking into account the neutron background event rate measured in the second phase, we obtained an event rate of (0.77 ± 0.08) evt/ day, corresponding to a flux inside the laboratory $\Phi = (4.0 \pm 1.0) \times 10^{-6}$ neut/ s/ cm^2, for neutrons energies between 2 and 6 MeV.

5. Origin of neutrons

5.1 Chemical and elemental composition of the rock in the L.S.M.

The L.S.M. rock is constituted of glossy schist. Rock samples have been analysed by spectrometry, by the "Département de Géologie et Océanographie de l'Université Bordeaux1", to determine the chemical composition of each element and their corresponding abundance by weight (Table 2 and 3) [14]. The uranium and thorium content of the rocks at the underground site has also been measured (Table 4), with a germanium detector of 100 cm^3 [14].

	SiO_2	Al_2O_3	Fe_2O_3	MnO	MgO	CaO	TiO_2	K_2O	Na_2O	P_2O_5	Weight loss on ignition
Rock	14.9	5.0	2.8	0.038	1.4	42.8	0.12	0.25	0.6	0.15	31.5
Concrete	5.8	1.1	0.74	0.008	1.3	51.5	0.17	0.02	0.02	0.15	38.5

"Weight loss on ignition" is the loss of weight (H_2O, CO_2, ...) after heating at 1000 °C during few hours.

Table 2 : Major elements concentration (in %) of the L.S.M

	P	Cu	Ba	Zn	Ni	Zr	Rb	Sr	S	Pb	Cr	Nb	Cl	Ga
Rock	14.3	33.5	6.3	46.4	22.8	33.8	84.2	1046	2516	670	22.5	19.6	680	2.5
Con-crete	14.5	22	0.1	2323	8.3	13.2	74.1	463	4011	674	21.5	20.8	182	11.2

Table 3 : Minor elements concentration (in ppm or μg/g) of the L.S.M

	^{238}U	^{232}Th	^{40}K
Rock	(0.84 ± 0.2) ppm	(2.45 ± 0.2) ppm	(0.213 ± 0.03) Bq / g
Concrete	(1.9 ± 0.2) ppm	(1.4 ± 0.2) ppm	(7.73 ± 1.3) 10^{-2} Bq / g

Table 4 : Rock and concrete activity (in ppm and Bq/g) of the L.S.M

5.2 Neutrons sources

Neutrons present in the rock are those produced underground by cosmic muons (the only particles which cross the rock, down to a few hundred kilometers), and neutrons induced by spontaneous fission and (α,n) reactions due to uranium and thorium traces in the rock [7].

* Neutron production by cosmic muons

These neutrons are produced as a result of electromagnetic interactions of fast muons with nuclei in the rocks and by μ^- capture in the target nuclei. We studied these two processes in the L.S.M rock elements, and in the lead of the shield.

In the rock, one can calculate the number of emitted neutrons as a function of the muon stopping rate, the laboratory depth and the Z of the considered element [15]. At a depth of 4800 mwe, the neutron flux obtained with the different elements of the rock is $(2.30 \pm 0.50) \times 10^{-8}$ neut/ year/ g of rock.

In the lead, neutrons are produced by electromagnetic interaction. From Ref. [16], we estimated the product of the multiplicity by the neutron production cross section $m\bar{\sigma}$, at a depth of 4800 mwe. The neutron flux is $(3.2 \pm 0.2) \times 10^{-7}$ neut/ year/ g of lead of the shield.

We can conclude that neutron flux produced by muons interaction is negligible.

* Neutron production by spontaneous fission

Heavy elements present in the rock undergo spontaneous fission. Neutrons originating from the spontaneous fission of ^{235}U and ^{232}Th were ignored on the basis of their very long fission half-lifes compared with that of ^{238}U. Several authors have studied the neutron energy distribution emitted by spontaneous fission [17]. The shape of the neutron spectrum of ^{238}U turns out to be very close to a Maxwellian [18] :

$$N(E) = 0.452\sqrt{E}\ e^{-E/1.3} \qquad (1)$$

The average number of neutrons emitted per fission event is 2.4 ± 0.2 [19]. The number of spontaneous fission of ^{238}U is 0.218 / year/ g of rock for 1 ppm of uranium in the rock.

Figure 8 represents the neutron energy distribution due to spontaneous fission of ^{238}U in the rock. We obtained a neutron flux of 0.47 neut/ year/ g of rock, emitted by spontaneous fission in the rock.

* Neutron production by (α,n) reactions

Alpha-particles are emitted by uranium, thorium and their daughter products present in the rock. The yield of neutrons per α-particle depends on the (α,n) reaction cross-section (energy dependent) and on the energy loss of the α-particle in the rock components. We used the procedure and tables given in Ref. [20] to obtain the neutron yield and we calculated the neutron energy spectrum resulting from the (α,n) reactions.

The neutron energy is a function of the α energy, the reaction energy Q and the neutron emission angle. We supposed (for a given α energy) that the neutron is emitted at 90° (symmetric emission). (We also supposed that the residual nucleus is produced in its fundamental state).

Under these conditions, the neutron energy is given by :

$$E_n = \frac{MQ + E_\alpha (M - M_\alpha)}{M_n + M} \qquad (2)$$

M being the mass of the final nucleus.

From the ratio (Mass stopping power of each element) / (Linear stopping power for the total rock elements), we calculated the neutron rate emitted for each element. We obtained the neutrons global yield N, emitted by α-particle as a function of the α energy ($1 < E_\alpha < 9.8$ MeV). The neutron production rate dN/dEn per α-particle, as a function of the neutron energy, is represented in figure 9, element per element.

We take into account the neutrons produced by the α disintegration with α energies greater than 6 MeV, the reaction cross sections being negligible below this value. For the ^{238}U family, there were the disintegration of the ^{218}Po and ^{214} Po, and for the ^{232}Th the disintegration of the ^{220}Ra, ^{216}Po and ^{212}Po. Figure 10 represents the neutron energy distribution, obtained by (α,n) reactions. The neutron flux is 1.93 neut/ year/ g of rock, inside the rock.

Figure 11 presents the neutron energy distribution (spontaneous fission + (α,n) reactions) inside the rock.

5.3 Neutron spectrum and flux in the laboratory

A Monte-Carlo simulation of the L.S.M. (a parallelepiped of 10 x 11 x 30 m^3), with rock composition, showed that a thickness of 30 cm of rock is enough to decrease the neutron energy below 1 MeV. With the calculated spectrum of the rock (Fig. 11) entered in the simulation, we obtained the neutron spectrum in the laboratory (Fig. 12), above 1 MeV.

This spectrum corresponds to a neutron flux of 1×10^{-6} neut/ s/ cm^2 in the laboratory. The difference between this value and the experimental one (see 4.3) by a factor 4 can be explained by the difficulty to measure the H_2O contribution (see Table 2) in the rock. In spite of this uncertainty, we consider that this value is in reasonable agreement with the experiment result.

We can conclude that the main contribution to the neutron flux in the L.S.M comes from the rocky walls of the laboratory.

6. Thermal neutron flux measurement

To make a global survey of the neutron environment in the L.S.M, we have also measured the thermal neutron flux, using two Helium-3 detectors (this study is based on Ref. [7]). These detectors have cylindrical geometry with a length of 30 cm and a diameter of 2.5 cm. The filling gas consists of ^3He at a pressure of 4.00 bars. The detectors are surrounded by a polystyrene protection, and a Faraday cage. The thermal neutron sensitivity of these detectors is $s = 48$ counts/ sec. n. cm^2.

The energy calibration of the analyser was carried out using the position of the thermal peak at 764 keV using an Am-Be neutron source. There were three consecutive periods of 45 days each.

- first period : the two detectors were installed inside a Faraday cage.
- second period : the two detectors were installed inside the lead and copper shielding of the previous fast neutron experiment, with wax protection around the shielding.
- third phase : the two detectors have been installed in the Faraday cage, with a cadmium sheet around each detector (to stop the low energy neutrons).

We obtained the background from the second period. The thermal and epithermal flux are negligible in this case.

We have used the cadmium difference method [7], as described hereafter. The counting rate due to thermal neutrons is given by :

$$C_{th} = (C_1 - C_2) - F_{Cd}\,(C_3 - C_2) \qquad (3)$$

C_{th} is the true rate due to thermal neutrons. C_1, C_2 and C_3 are the counting rate in the phase 1, 2 and 3. F_{Cd} is a cadmium correction factor which takes into account the fact that cadmium captures neutron between the "cut-off" energy of the epithermal spectrum (≈ 0.1 eV) and the "cadmium cut-off" energy E_{Cd}. For our experimental situation, the appropriate values are $F_{Cd} = 2.6$ and $E_{Cd} = 0.63$ eV [21]. We obtained $C_{th} = 7.5 \times 10^{-5}$ neut/ s per detector. Thus the flux is : $\Phi_{th} = (1.6 \pm 0.1) \times 10^{-6}$ neut/ s/ cm^2

This flux can be compared with other experiments as shown in Table 5.

Thermal neutron flux (cm^{-2} s^{-1})	Reference
$(2.05 \pm 0.06) \times 10^{-6}$	[22]
$(1.08 \pm 0.02) \times 10^{-6}$	[23]
$(1.94 \pm 0.11) \times 10^{-5}$	[7]

Table 5 : Thermal neutron flux

7. Conclusion

We have measured a fast neutron flux of $(4.0 \pm 1.0) \times 10^{-6}$ neut/ s/ cm^2 at a depth of 4800 mwe in the L.S.M. The neutron energy distribution with a threshold at 1 MeV is concentrated around 3 MeV. These neutrons come mainly from the uranium and thorium traces in the rock.

This flux is compatible with the estimations which can be made from the spontaneous fiission and the (α,n) reactions induced in the walls of the cavity by the traces of α emitters. The knowledge of the magnitude as well as the energy distribution of the neutron flux will be very useful for the low background experiments planned in the Modane laboratory.

The thermal neutron flux has been measured to be $(1.6 \pm 0.1) \times 10^{-6}$ neut/ s/ cm^2.

Acknowledgements

We would like to thank Philippe HUBERT of the CENBG of Bordeaux for the L.S.M rock analysis and profitable discussions. We are also grateful to the L.S.M. technical team the help of which was essential during the different phases of the data taking, in particular Philippe CHARVIN.

References

[1] C. Alcock et al., Nature 365 (1993) 621
E. Aubourg et al., Nature 365 (1993) 623
A. Udalski et al., Astrophys. J. L69 (1994) 426
R. Ansari et al., Nucl. Phys. B (proc. suppl.) 43 (1995) 165

[2] M. W. Goodman and E. Witten, Phys. Rev. D 31 (1985) 3059
G. B. Gelmini et al., Nucl. Phys. B 351 (1991) 623
A. Bottino et al., Astrop. Phys. 2 (1994) 67

[3] A. de Bellefon et al., Astrop. Phys. Vol 6/1 (1996) 35

[4] G. Jungman, M. Kamionkowski and K. Griest, Physics Reports Vol 267 n°5, 6 (1996) 195

[5] C. Berger et al., N.I.M. A 262 (1987) 463

[6] A. Rindi et al., N.I.M. A272 (1988) 871

[7] S. R. Hashemi-Nezhad and L. S. Peak, N.I.M. A 357 (1995) 524

[8] M. Abbes et al., N.I.M. A 374 (1996) 164

[9] C. N. Chou, Phys. Rev. 87 (1952) 904

[10] B. A. Pohl et al., Lawrence Radiation Laboratory, Livermore (1969)
R. L. Craun et al., N.I.M. 80 (1970) 239
R. A. Cecil et al., N.I.M. 161 (1979) 439
Y. Uwamino et al., N.I.M. 204 (1982) 179

[11] Application Software Group, CERN Program Library Long Writeup W5013, CERN (1993)

[12] V. Chazal, thesis Université Lyon1 n° 176-96 (1996)

[13] H. de Kerret and B. Lefièvre, Simulation des neutrons de basse énergie par Monte Carlo, Collège de France, LPC 88-01

[14] P. Hubert, Private communication

[15] S. Charalambus, Nucl. Phys. A 166 (1971) 145
T. Kozlowski et al., Nucl. Phys. A 436 (1985) 717

[16] L. Bergamasco et al., Il Nuevo Cimento, V.13A n°2 (1973) 403
O. C. Allkofer et al., Nucl. Phys. B8 (1968) 402

[17] N. Nereson, Phys. Rev. 85 (1952) 600
D. B. Nicodemus and H. H. Staub, Phys. Rev. 89 (1953) 1288

[18] B. E. Watt, Phys. Rev. 87 (1952) 1037

[19] D. J. Littler, Proc. Phys. Soc. London A 64 (1951) 638; A 65 (1952) 203

[20] J. H. Gibbons and R. L. Macklin, Phys. Rev. V114 n°2 (1959) 571
Y. Feige et al., J. Geophys. Res. 73 (1968) 3135
J. K. Bair and J. Gomez del Campo, Nucl. Sc. & Eng. 71 (1979) 18
C. W. Cheng and J. D. King, J. Phys. V5 n°9 (1979) 1261
R. Heaton et al., N.I.M. A 276 (1989) 529
R. Heaton et al., Nucl. Geophys. V4 n°4 (1990) 499

[21] K. H. Beckurts and K. Wirtz, Neutron Physics (Springer, Heidelberg, 1964) pp. 273 - 279

[22] A. Ridi et al., N.I.M. A 272 (1988) 871

[23] P. Belli et al., Nuovo Cimento A 101 (1989) 959

Figure captions

Fig. 1 : A schematic view of the detection principle

Fig. 2 : Q_2/Q_1 ratio of the prompt events obtained with Am - Be source

Fig. 3 : Scintillation response of NE320, compared to various organic scintillators

Fig. 4 : Expected spectrum of the ratio R_{PSD} versus Total charge Q_1, for the prompt pulses (a) and delayed pulses (b). In addition in (b), energy (in electron equivalent) of the (α + t) events.

Fig. 5 : Time distribution for the first experimental phase (lead + copper) and second experimental phase (wax + lead + copper).

Fig. 6 : Experimental neutron energy spectrum, in electron equivalent energy, for the first and second phase.

Fig . 7 : Estimated neutron energy spectrum, in the laboratory.

Fig. 8 : Neutron energy distribution obtained by spontaneous fission of ^{238}U in the rock.

Fig. 9 : Neutron production rate dN/dE_n per α - particule, element per element, obtained as a function of neutron energy.

Fig. 10 : Neutron energy distribution obtained by (α,n) reaction in the rock.

Fig. 11 : Neutron energy distribution in the rock, from the spontaneous fission contribution plus (α,n) reactions contribution.

Fig. 12 : Simulation of the neutron spectrum in the laboratory above 1 MeV.

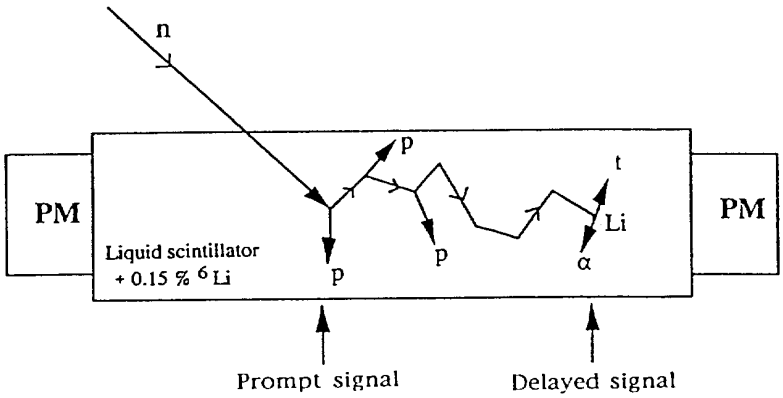

Fig. 1. A schematic view of the detection principle.

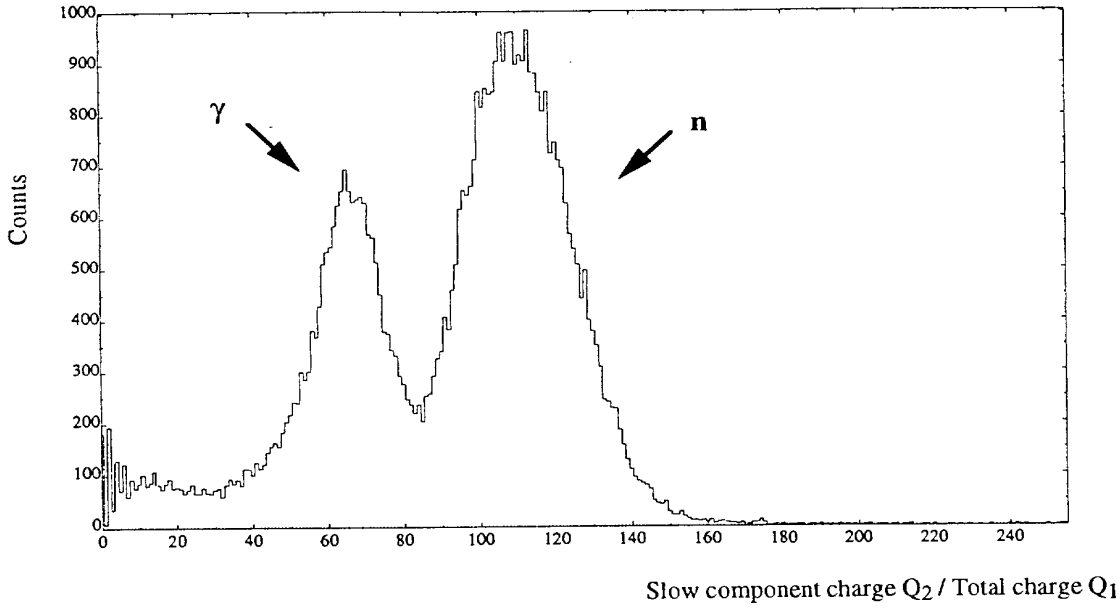

Fig. 2. Q_2 / Q_1 ratio of the prompt events obtained with an Am - Be source.

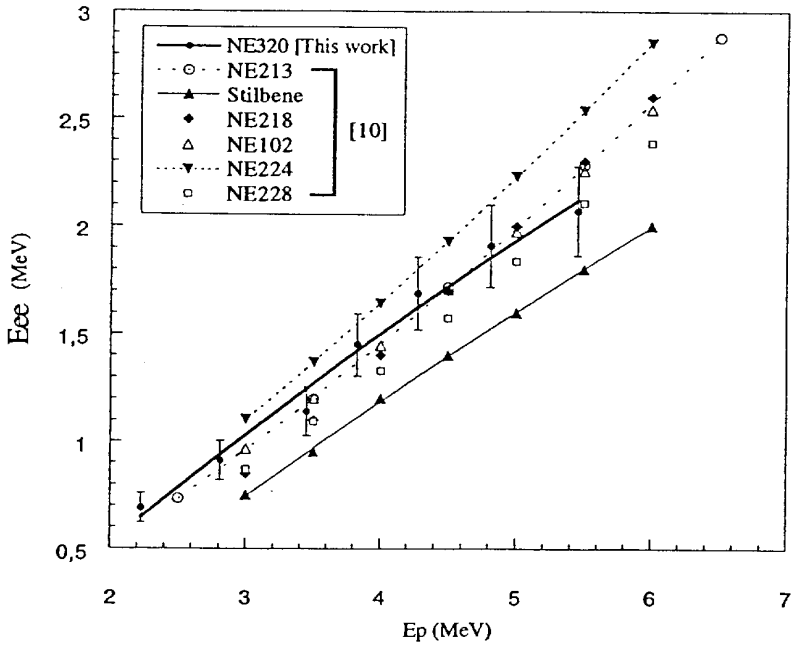

Fig. 3. Scintillation response of NE320, compared to various organic scintillators.

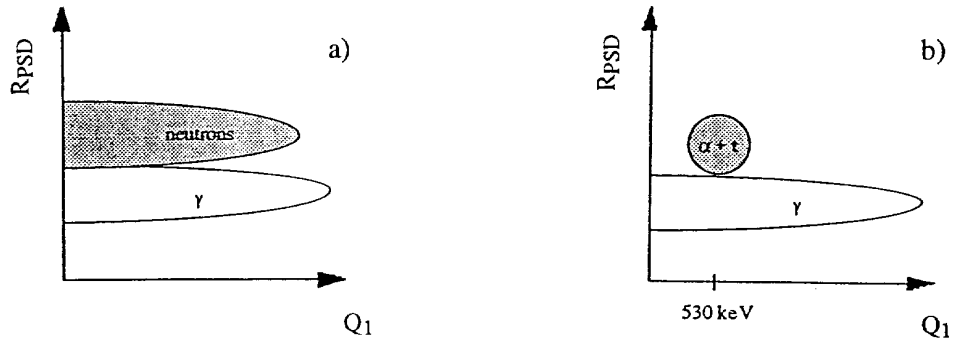

Fig. 4. Expected spectrum of the ratio R_{PSD} versus Total charge Q_1, for the prompt pulses (a) and delayed pulses (b). In addition in (b), energy (in electron equivalent) of the (α+t) events.

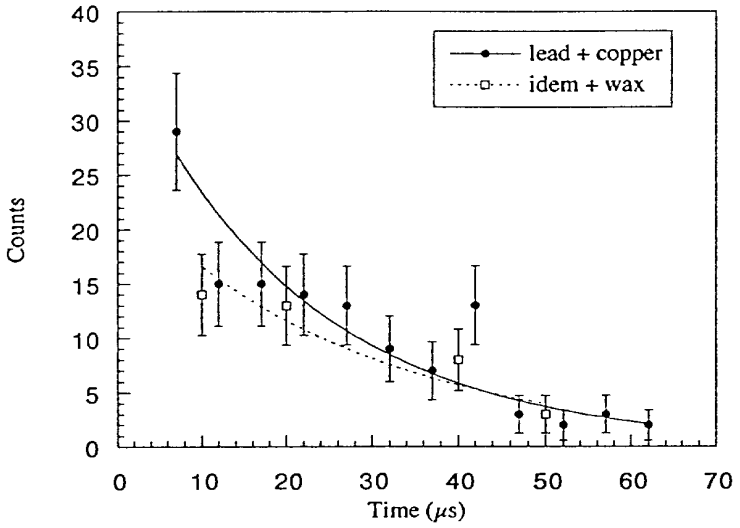

Fig. 5. Time distribution for the first experimental phase (lead + copper) and second experimental phase (wax + lead + copper).

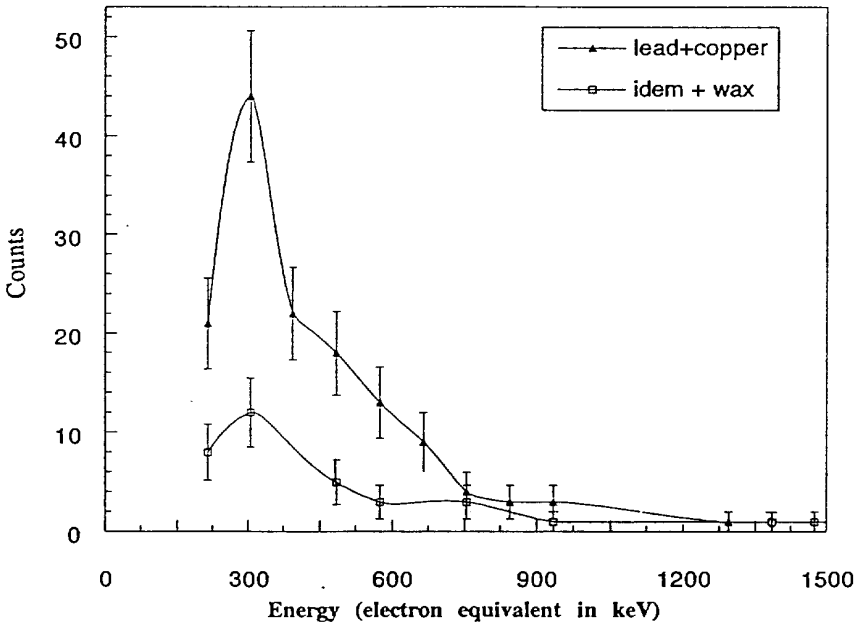

Fig. 6. Experimental neutron energy spectrum, in electron equivalent energy, for the first and second phase.

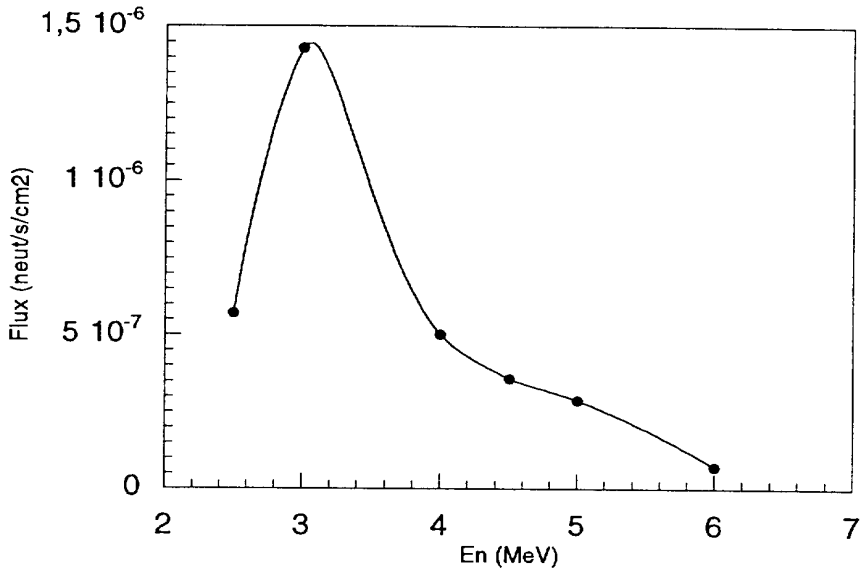

Fig. 7. Estimated neutron energy spectrum, in the laboratory.

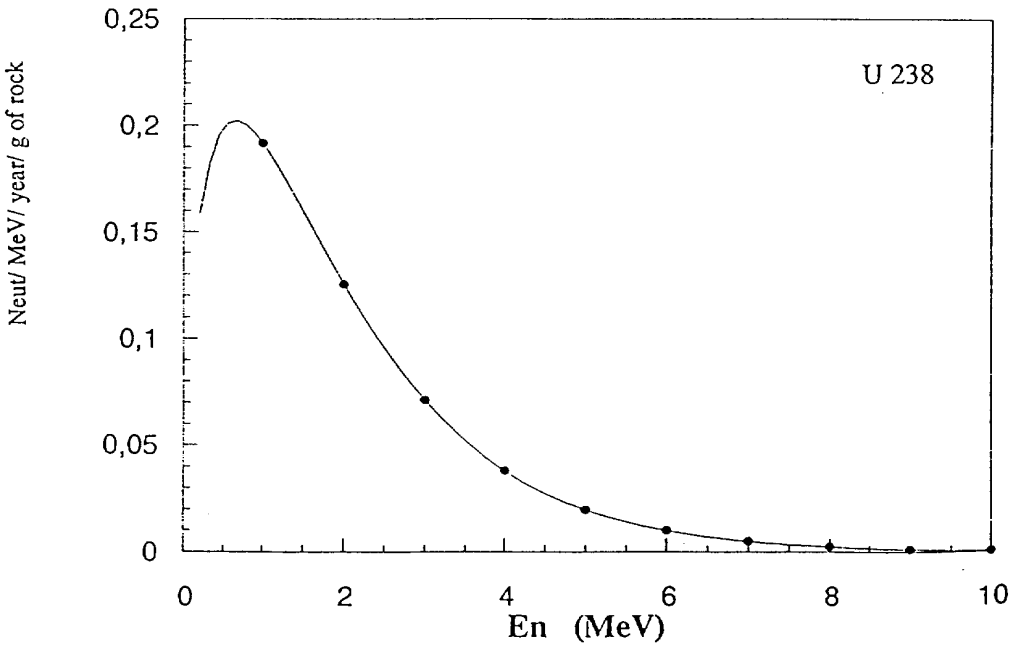

Fig. 8. Neutron energy distribution obtained by spontaneous fission of ^{238}U in the rock.

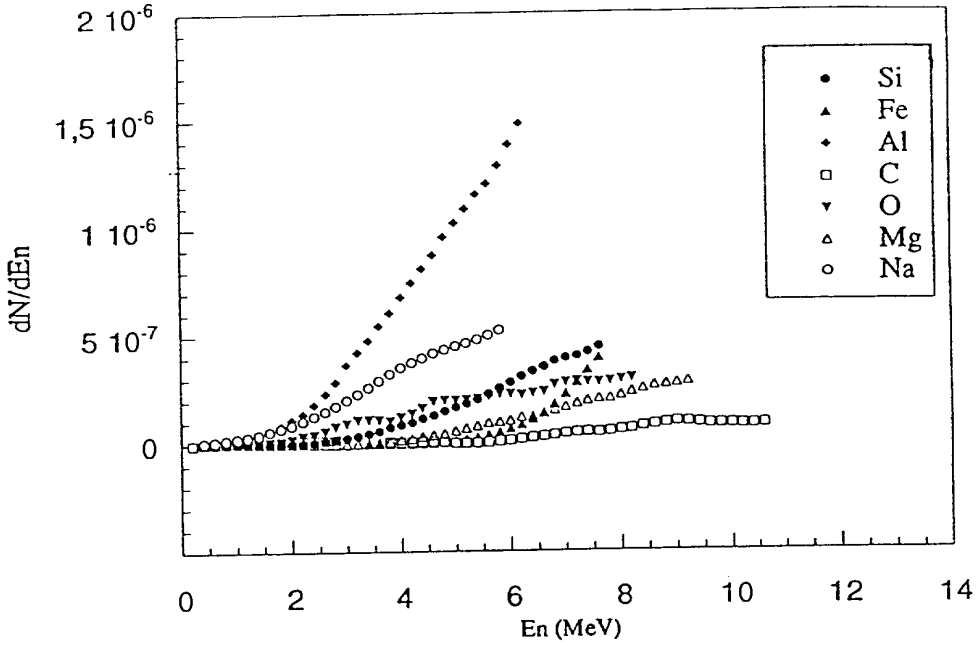

Fig.9. Neutron production rate dN / dE_n per α-particle, element per element, obtained as a function of neutron energy.

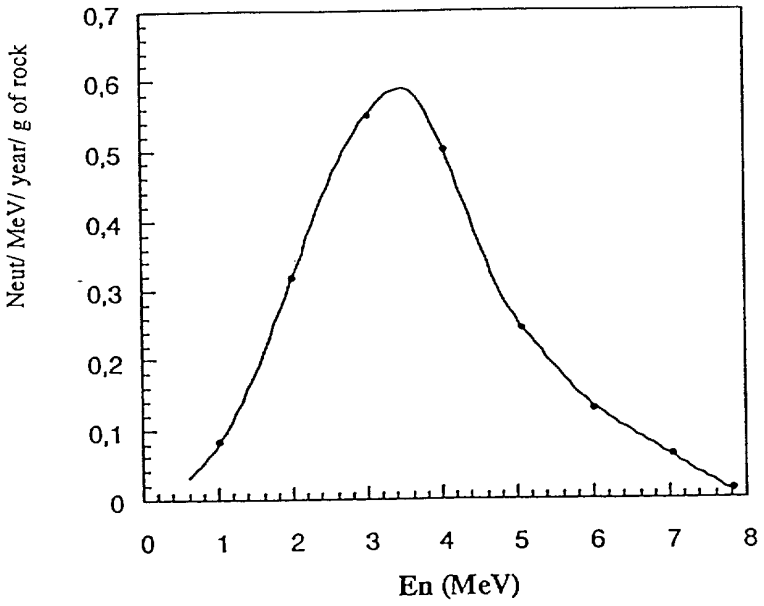

Fig. 10. Neutron energy distribution obtained by (α,n) reactions in the rock.

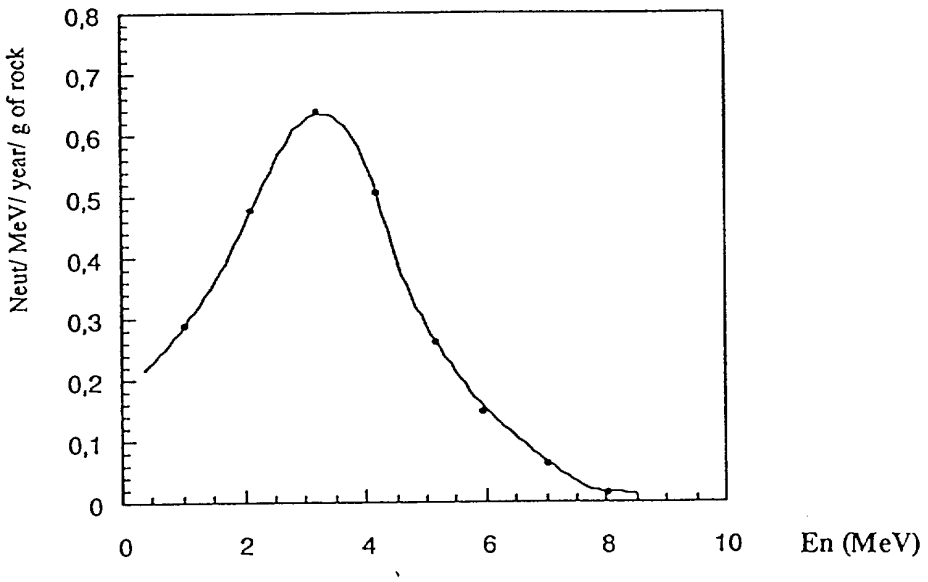

Fig. 11. Neutron energy distribution in the rock, from the spontaneous fission contribution plus the (α,n) reactions contribution.

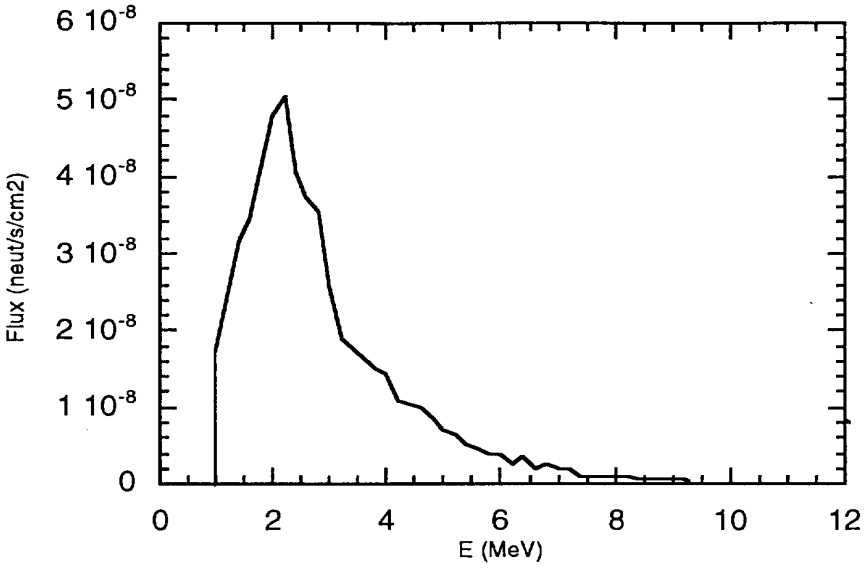

Fig. 12. Simulation of the neutron spectrum in the laboratory above 1 MeV.